

# Robust quantum computing on qubit arrays with fixed coupling

Nguyen H. Le,<sup>1</sup> Max Cykiert,<sup>1</sup> and Eran Ginossar<sup>1</sup>

<sup>1</sup>*Advanced Technology Institute and Department of Physics,  
University of Surrey, Guildford GU2 7XH, United Kingdom*

We show how robust and scalable quantum computing can be realized on an arbitrarily large two dimensional arrays of qubits with fixed longitudinal couplings despite significant uncertainty in all the qubit-qubit and drive-qubit coupling strengths. This opens the possibility for bypassing the fabrication complexity associated with tunable couplers required in conventional quantum computing hardware. Our approach is based on driving a chosen subarray of qubits such that the total multi-qubit Hamiltonian can be decomposed into a sum of commuting few-qubit blocks and on efficient optimization of the unitary evolution within each block. Robust optimal control is then employed to implement a universal set of quantum gates with fidelities around 99.99% despite 1% uncertainty in the Hamiltonian's parameters. This robust feature is crucial for scaling up as uncertainty in the properties of qubits is substantial in large devices.

Great progress has been achieved recently in various physical platforms for quantum computing, most notably is the 54-qubit programmable superconducting processor [1]. High fidelity two-qubit gates were also demonstrated for trapped ions [2], neutral atoms in optical tweezers [3], and spin qubits in silicon [4, 5] and GaAs [6]. These experimental implementations are based on tunable coupling between qubits where the interaction is switched on only when the two qubit gates are implemented. In solid state quantum computers, tunable couplers typically involve more circuit elements and require their own external control for tuning the magnitude of the interaction [1, 4, 7] leading to overheads in fabrication and wiring. For solving real-world problems, a quantum computer need a large number of qubits [8], and the complexity of the tunable couplers adds to the technological difficulties in scaling up the device. In contrast, fixed couplers, such as capacitive coupling between superconducting qubits [9], do not require the extra components for controlling the magnitude of the interaction, resulting in a substantial simplification of hardware architecture. In many platforms fixed coupling comes from natural interactions, for example the mutual induction between concentric transmons [10], exchange between spins [11] and dipole-dipole interaction between atoms [3], and hence no parts are necessary for coupling the qubits. Another challenge in scaling up is the uncertainty in the physical parameters of the qubits due to variability in fabrication and fluctuating stray fields. Precise characterisation and calibration of every qubits is impractical in large devices, and hence it is crucial to have quantum operations that are robust against uncertainty.

In this paper we show that one can use external drives to implement robust and scalable quantum computing on an array of qubits with fixed longitudinal qubit-qubit interactions, opening an alternative pathway for quantum computer hardware architecture. By robust we refer to the high fidelity of the quantum gates despite the uncertainty associated with the system parameters across the array. In general the fixed interaction entangles all the qubits constantly in a non-controllable way. We find that, by driving a subset of the qubits one can: 1) effectively

remove the entangling to apply a single-qubit gate, no gate (identity), or exploit the entangling to apply a target two-qubit gate, and 2) realize the gates with fidelities around 99.99% which are robust against 1% uncertainty in all the qubit-qubit and drive-qubit couplings. The effect of the uncertainty in the detuning is also considered although it is typically much smaller. The robustness of the fidelity against uncertainties is crucial for an architecture with entirely fixed couplers because calibrating a qubit or qubit pair is more challenging. A particularly important quantum gate in our scheme is an active identity gate which keeps the state of a subset of qubits unchanged. In an implementation of a quantum circuit any idle interval between gates has to be filled with this identity gate to prevent the non-controllable evolution caused by the fixed interactions.

Our results are scalable based on the observation that the system's Hamiltonian can be decomposed into commuting blocks of only a few qubits. Each block has a low dimensional Hilbert space and a small number of uncertain parameters, and thus its unitary evolution can be optimized efficiently using robust optimal control algorithms [12–17]. This decomposition exists when the qubit-qubit coupling term is diagonal in the computational basis, for example the ZZ interaction, and when only a subarray of qubits, chosen based on the quantum gate of interest, is driven, as demonstrated in Fig. 1. The choice of driven subarray must also satisfy the following requirement for making the gates robust against uncertainty in all the qubit-qubit couplings: every undriven qubit must be coupled to at least one driven qubit (see more details below). Our scheme relies on the individual control of each qubit with external drive, already available in all quantum computing architectures for implementing single qubit gates, and thus does not require additional structures.

We consider a system of qubits coupled by fixed nearest-neighbor longitudinal interaction, i.e., an interaction that commutes with the bare qubit's Hamiltonian. For simplicity we choose the ZZ interaction, for which there has been active theoretical and experimental progress recently with superconducting qubits [18–21].

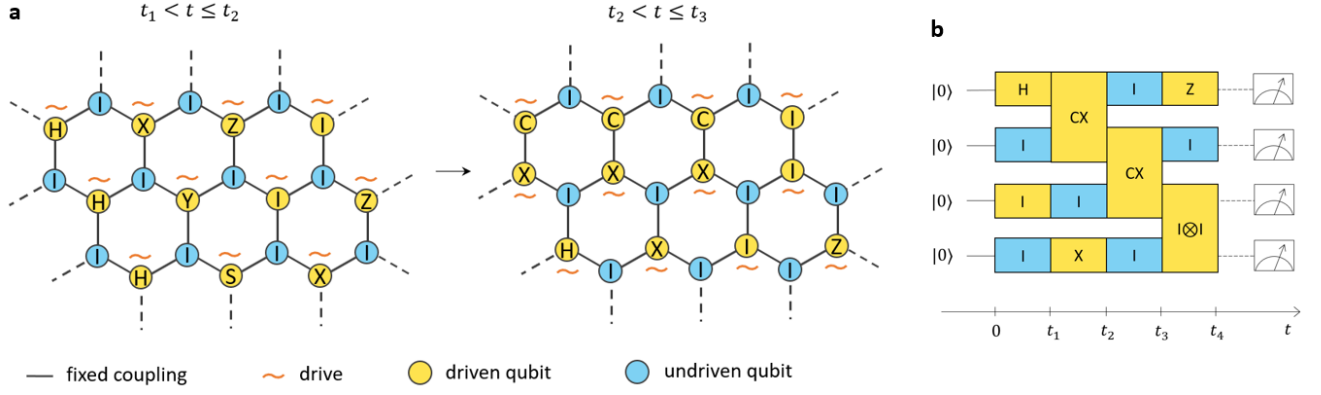


FIG. 1. a) An example of implementing quantum gates on an array of qubits with fixed couplings. In any given step only a subarray can be driven. This subarray must satisfy specific requirements so that the array’s Hamiltonian can be decomposed into commuting few-qubit blocks, and that the quantum gates are robust against uncertainty in all parameters of the Hamiltonian (see text). Each drive can implement a gate on the driven qubit, and through its combination with the fixed qubit-qubit couplings also implements an identity gate on the neighboring undriven qubits. In the next step a different subarray is driven for implementing gates on a different set of qubits. Here CX on two adjacent qubits denotes the CNOT gate and I the identity gate. b) Illustration of a quantum circuit in our scheme. The key feature is that any idle interval between gates must be filled with an active identity gate, for preventing unwanted evolution due to the fixed couplings.

When a subset of qubits is driven by external fields, the system’s Hamiltonian is

$$\mathcal{H}(t) = - \sum_j \frac{\omega_j}{2} \sigma_j^z + \sum_{j \in \mathcal{L}} d_j E_j(t) \sigma_j^x + \sum_{jk} J_{jk} \sigma_j^z \sigma_k^z,$$

$$E_j(t) = E_j^x(t) \cos(\nu_j t) + E_j^y(t) \sin(\nu_j t),$$

where  $\nu_j$  is the frequency of the drive on the  $j$ -th qubit,  $E_j^x(t)$  and  $E_j^y(t)$  the two quadratures of the field,  $d_j$  the  $j$ -th qubit’s dipole matrix element, and  $\mathcal{L}$  the driven subset. Typically the qubit’s transition energy,  $\omega_j$ , is much larger than the interaction,  $J_{jk}$ , and hence  $|0, 0, \dots, 0\rangle$  is the ground state of the undriven Hamiltonian and can be initialised by cooling.

In the frame rotating with the qubits’ frequencies, described by the unitary transformation  $U_0(t) = e^{i \sum_j \frac{\omega_j}{2} \sigma_j^z t}$ , the Hamiltonian in the rotating wave approximation is

$$H(t) \approx \sum_{j \in \mathcal{L}} \frac{1}{2} [\Omega_j(t) \sigma_j^x + \Omega'_j(t) \sigma_j^y] + \sum_{jk} J_{jk} \sigma_j^z \sigma_k^z, \quad (1)$$

where

$$\Omega_j(t) = \Omega_j^x(t) \cos(\delta_j t) + \Omega_j^y(t) \sin(\delta_j t),$$

$$\Omega'_j(t) = \Omega_j^y(t) \cos(\delta_j t) - \Omega_j^x(t) \sin(\delta_j t). \quad (2)$$

Here,  $\Omega_j^{x,y}(t) \equiv d_j E_j^{x,y}(t)$  is the Rabi frequency and  $\delta_j \equiv \nu_j - \omega_j$  is the detuning.

Computing the unitary evolution of a many-body Hamiltonian like  $H(t)$  is in general intractable due to the exponential complexity of the wave function, unless one can decompose the Hamiltonian into a sum commuting few-qubit blocks, i.e.,  $H(t) = \sum_l H_l(t)$ , where all the  $H_l(t)$  are mutually commuting. The unitary evolution

after a time duration  $T$  is then  $U(T) = \prod_l U_l(T)$  where  $U_l(T) = \mathcal{T} e^{-i \int_0^T dt' H_l(t')}$  and  $\mathcal{T}$  is the time-ordering operator.  $U_l(T)$  can be efficiently computed since it involves only a few qubits. The  $U_l(T)$  factors are also mutually commuting and can be seen as *parallel* quantum gates applied on separate qubit blocks.

We derive a pattern of driving that enables the decomposition of  $H(t)$  into few-qubit commuting blocks. The driving pattern must also allow using optimal control to make the final unitary robust against the uncertainties in the qubit-qubit and drive-qubit coupling. We consider an arbitrarily large honeycomb array of qubits with nearest neighbor ZZ coupling and an alternating pattern where only the subarray colored in yellow in Fig. 2a is driven, then  $H(t) = \sum_{j \in \mathcal{L}} H_j(t)$  where  $\mathcal{L}$  is the driven subarray and

$$H_j(t) = \frac{1}{2} [\Omega_j(t) \sigma_j^x + \Omega'_j(t) \sigma_j^y] + \sum_{k \in \text{NB}_j} J_{jk} \sigma_j^z \sigma_k^z, \quad (3)$$

where  $\text{NB}_j$  is the set of the three nearest neighbors of qubit  $j$ . Each of the building block  $H_j$  involves four qubits and they commute with each other. This can be seen in a more transparent way by a graphical representation of the Hamiltonian in Fig. 2a. Each link in the graph represents a ZZ coupling term; a yellow vertex represents a single-qubit driving term, and a cyan vertex represents an undriven qubit and hence adds nothing to  $H(t)$ . All the ZZ terms commute with each other, and a driven vertex does not commute with only the three links connecting to it, because  $\sigma^x$  and  $\sigma^y$  does not commute with  $\sigma^z$ . Thus, the total Hamiltonian can be expressed as a sum of commuting four-qubit blocks enclosed by the dash circles in Fig. 2a. Each block has only one driven qubit in the center. The qubit at the intersection of two

neighboring blocks must not be driven for the commutativity to hold. We show later on that it is possible to implement a robust single-qubit gate on the driven qubits without changing the state of the undriven qubits despite the permanent ZZ interaction in the block.

In a conventional device with tunable couplers the interaction is turned on only when a two-qubit entangling gate is needed [21]. In our case the ZZ coupling is always on, and in general it entangles all the qubits at all time. However, we find that it is still possible to implement a specific two-qubit entangling gate, for example the CNOT gate, between two targeted qubits by driving both of them (more details below). Turning on the drives on two neighboring qubits results in the pattern of Fig. 2b where the central row is built from identical six-qubit blocks. The rest of the array can be driven as before.

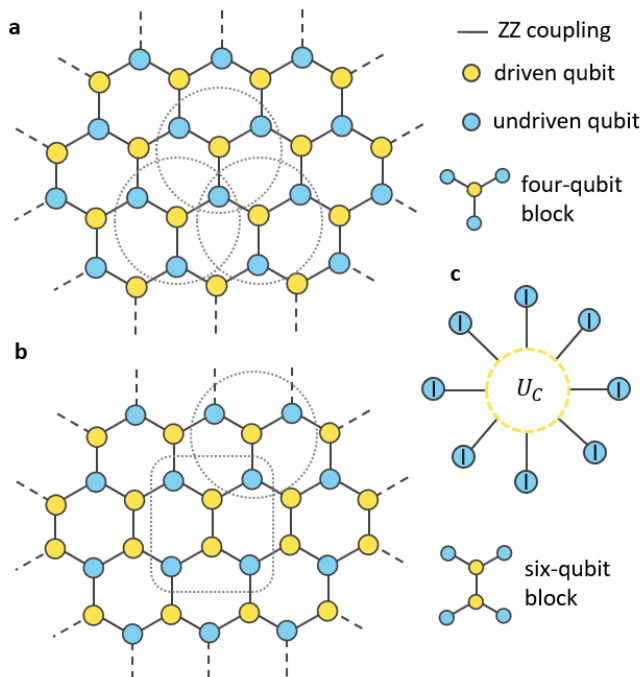


FIG. 2. a) An arbitrarily large 2D array of coupled qubits in a honeycomb array. Each link represent a ZZ coupling term. A yellow (cyan) vertex represents a driven (undriven) qubit. The total Hamiltonian can be decomposed into a sum of identical four-qubit blocks that commute with each other (enclosed in the dashed circles). An undriven qubit is shared by three neighboring blocks. (b) The pattern of driving for implementing a two-qubit gate, resulting in a central row of identical six-qubit blocks (enclosed by the dashed rectangle). The rest of the array can be decomposed into the four-qubit block in (a). (c) A star graph with undriven qubits on the boundary and a driven subset of one or more qubits in the center. Every undriven qubit must be connected to at least one driven qubit. By utilizing optimal control on the driven subset it is possible to apply a unitary of the form  $U_C \otimes I_B$  where  $U_C$  is a target unitary on the central driven subset, and  $I_B \equiv | \otimes | \otimes \dots \otimes |$  is the identity in the Hilbert space of the undriven qubits on the boundary (see text).

The reader may wonder why the six-qubit blocks are required for the entire central row when only one two-qubit gate is needed. This is to satisfy a *condition for robust control*: Every link (ZZ term) must be connected to at least one driven qubit, and the pattern in Fig. 2b is the simplest we can find. If a link,  $J_{jk}\sigma_j^z\sigma_k^z$ , is not connected to any driven qubit, then it commutes with every other terms in the Hamiltonian, and its contribution to the total unitary evolution is simply the factor  $e^{-iJ_{jk}\sigma_j^z\sigma_k^z T}$ , which cannot be made robust against uncertainty in  $J_{jk}$  due to the absence of control.

Our claim of robust quantum computing lies in the key numerical finding that, for a star graph where the undriven qubits on the boundary are connected to a central subset of driven qubits (see Fig. 2c), it is possible to realize an operation of the type  $U_C \otimes I_B$  where  $U_C$  is a unitary acting on the driven subset, and  $I_B$  is the identity matrix acting on the undriven subset at the boundary. This means that the gate  $U_C$  is applied to the driven subset while the rest remains undisturbed. Obviously these qubits on the boundary are acted on by the ZZ interactions during the gate, but we find that by choosing the right pulse shape one can use the combined effect of the central driving terms and the ZZ connectors to ensure that the identity is applied to the boundary at the end of the pulse. Therefore, the ZZ interactions are effectively removed in a stroboscopic fashion. If the driven subset has one (two) qubit,  $U_C$  is a single-qubit (two-qubit) gate. Moreover, we find that  $U_C \otimes I_B$  can be realized with high fidelity despite significant uncertainty in all the ZZ couplings,  $J_j$ , all drive-qubit Rabi couplings,  $\Omega_j^{x,y}$ , and all the detunings,  $\delta_j$ , in the graph's Hamiltonian. The four and six-qubit blocks of Figs. 2 are star graphs with one and two driven qubits in the center, respectively. An implementation of quantum computation on the array is demonstrated in Fig. 1 where the driving subarray is shifted from one step to the next to apply the target quantum gate on the right qubits. If there is not gate on a qubit in a given step one applies the active identity gate to keep the state of this qubit unchanged.

In robust optimal control we divide the pulse duration,  $T$ , into  $M$  time bins of interval  $\Delta t$ . In each time bin the field amplitudes are kept constant. The set of the Rabi frequencies form the control vector,  $\mathbf{c} = \{\Omega_{jn}^\mu : 1 \leq n \leq M; \mu = x, y; j \in \mathcal{C}\}$ , where  $\mathcal{C}$  is the driven subset. The unitary evolution  $U_G(T)$  of the star graph  $\mathcal{G}$  is then a function of  $\mathbf{c}$ . Each qubit-qubit coupling,  $J_{jk}$ , and detuning,  $\delta_j$ , is allowed to vary independently in the uncertainty intervals  $[\bar{J} - \Delta J/2, \bar{J} + \Delta J/2]$ , and  $[\bar{\delta} - \Delta\delta/2, \bar{\delta} + \Delta\delta/2]$ , respectively. The uncertainty in the Rabi frequencies can be caused by that in the dipole-matrix elements, or a slow drift in the drive leading to changes in the field amplitudes from one experiment to the next [22]. This can be modelled by replacing  $\Omega_j^{x,y}(t)$  in  $H_G$  by  $\alpha_j \Omega_j^{x,y}(t)$  where  $\alpha_j$  is a dimensionless parameter that varies in the interval  $[1 - \Delta\alpha/2, 1 + \Delta\alpha/2]$ . Now the unitary  $U_G(T)$  also depends on  $J_{jk}$ ,  $\alpha_j$ , and  $\delta_j$ . The qubit-qubit couplings and dipole-matrix elements have

to be measured or estimated at the point of fabrication, thus their values can change substantially after the array was built. In contrast, it is possible to determine the frequency of every qubit in the completed array with typically very precise spectroscopic measurement. In the array the resonant frequency of each qubit is shifted due to the ZZ interactions, but we find a procedure of one and two-photon absorption measurements that can be combined to cancel these shifts and obtain the bare qubit frequency,  $\omega_j$  (see Appendix). Thus, in this paper we assume that the driving fields are tuned to resonance,  $\delta = 0$ , with residual uncertainties that are much smaller than the average qubit-qubit interaction,  $\Delta\delta_j/\bar{J} = 0.1\%$ . This small detuning uncertainty is easily achievable in most physical realizations of qubits owing to highly accurate spectroscopic measurement and excellent qubit's frequency stability [23].

Denote the set of these uncertain parameters as  $\mathbf{v}$ , then the robust optimal control problem can be defined as a max-min optimization problem: We find an optimal control that maximizes the minimum fidelity over  $\mathbf{v}$ ,

$$\mathcal{F}_{\max} = \max_{\mathbf{c}} \mathcal{F}(\mathbf{c}), \quad \mathcal{F}(\mathbf{c}) = \min_{\mathbf{v} \in \mathcal{V}} F(\mathbf{c}, \mathbf{v}), \quad (4)$$

where  $\mathcal{V}$  is the hypercube containing the possible values of  $\mathbf{v}$ , and  $F(\mathbf{c}, \mathbf{v})$  the fidelity based on the trace distance

$$F(\mathbf{c}, \mathbf{v}) = \left| \frac{1}{D} \text{tr} \left[ U_{\mathcal{G}}^\dagger(T) (U_{\mathcal{C}} \otimes I_{\mathcal{B}}) \right] \right|^2, \quad (5)$$

where  $D$  is the dimension of the Hilbert space of  $\mathcal{G}$ ,  $I_{\mathcal{B}}$  the identity matrix of the subset of undriven qubits on the boundary, and  $U_{\mathcal{C}}$  the target unitary that we want to apply on the central driven subset. In numerical computation one chooses a set of sampling points,  $\mathbf{v}_i$ , in  $\mathcal{V}$ , and find the minimum fidelity in this set. We found that when the uncertainties are all smaller than 5% and  $F(\mathbf{c}, \mathbf{v})$  is larger than 99% its minimum over  $\mathbf{v}$  always lies at one of the extreme points of  $\mathcal{V}$ , i.e., one of the corners of the hypercube. Thus we can redefine  $\mathcal{F}(\mathbf{c}) \equiv \min_{\mathbf{v}_i \in \mathcal{X}} F(\mathbf{c}, \mathbf{v}_i)$  where  $\mathcal{X}$  is the discrete set of the extreme points of  $\mathcal{V}$ . This drastically reduces the number of sampling points where  $F(\mathbf{c}, \mathbf{v})$  has to be computed. There are  $2^{n_u}$  extreme points in a hypercube of  $n_u$  uncertain parameters. For example, the 6-qubit block in Fig. 2b has 9 uncertain parameters, five  $J$ s, two  $\alpha$ s, and two  $\delta$ s, so we need to compute  $2^9 \equiv 512$  values of  $F(\mathbf{c}, \mathbf{v}_i)$  for any given  $\mathbf{c}$ .

We develop a numerical computation for gradient-based robust optimal control that can handle systems with up to 12 qubits and multiple uncertain parameters. Starting with a random initial guess for  $\mathbf{c}$ , we use gradients to identify a step  $\delta\mathbf{c}$  to maximize  $\min_i \nabla_{\mathbf{c}} F(\mathbf{c}, \mathbf{v}_i) \cdot \delta\mathbf{c}$ , the first order increment, so that  $F(\mathbf{c}, \mathbf{v}_i)$  is increased for all  $\mathbf{v}_i$ . In this way  $\mathcal{F}(\mathbf{c})$ , the minimum fidelity over  $\mathbf{v}_i$ , can be increased to a value very close to one. In practice we find that one can also raise  $\mathcal{F}(\mathbf{c})$  by maximizing the average fidelity,  $\sum_{i=1}^{n_{\mathcal{X}}} F(\mathbf{c}, \mathbf{v}_i)/n_{\mathcal{X}}$ , with gradient ascent, which in some cases works faster than trying to increase  $F(\mathbf{c}, \mathbf{v}_i)$  for all  $\mathbf{v}_i$ . For the  $n$ -th time bin

the time evolution is calculated by the mid-point rule  $e^{-iH_{\mathcal{G}}(t_n - \Delta t/2)\Delta t} + O(\Delta t^3)$  which is accurate when the time step is small. The matrix exponentiation is sped up by using sparse matrices, and the gradient computed from a simple and efficient second-order formula [24].

For the four-qubit block of Fig. 2a we derive optimal pulses to realize  $U_{\mathcal{C}} \otimes I_{\mathcal{B}}$  where  $U_{\mathcal{C}}$  is the Hadamard and  $\pi/8$  gates [25]. And for the six-qubit block of Fig. 2b we want  $U_{\mathcal{C}}$  to be the CNOT gate. These three gates form a universal set where any multi-qubit unitary can be approximated from with arbitrary precision [25], allowing universal quantum computing on the array. For a system with exclusively fixed coupling it is also necessary to implement the identity gate that keeps all the qubits in a block unchanged despite the permanent interaction.

In Table I we show the robust fidelities obtained for the universal set and the identity gates at various levels of uncertainty. The gate duration is divided into  $M = 100$  time bins. For 1% uncertainty the fidelity is higher than 99.999% for the single-qubit gates and exceeds 99.98% for the two-qubit gates. Even if the uncertainty is as high as 5% five-nines fidelities are still achieved for the single-qubit gates, and above 99.94% for the two-qubit gates. This can be improved by increasing the number of initial guesses, relaxing the constraints or raising the number of control variables. An example of an optimal pulse shape is shown in Fig. 3. We choose  $T = 2\pi/\bar{J}$  but this specific value of the duration is not essential; the same order of magnitudes are achieved for the fidelities when  $T$  is changed by 10%. In order to see the effectiveness of robust optimal control we also calculate the fidelities with non-robust optimal control: We first neglect all the uncertainties and optimize the fidelity for the ideal case where  $J_j = \bar{J}$ ,  $\alpha_j = 1$  and  $\delta_j = 0$  for all  $j$ , then we use the obtained optimal control,  $\mathbf{c}_{\text{ideal}}$ , to calculate the minimum fidelity in the hypercube,  $\mathcal{F} = \min_{\mathbf{v} \in \mathcal{V}} F(\mathbf{c}_{\text{ideal}}, \mathbf{v})$ . The results are shown in the parentheses of Table I. robust optimization improves the fidelities by two to three nines when the uncertainties are significantly large (1% and 5%).

$\Delta J/\bar{J}$	$\Delta\alpha$	Had.	$\pi/8$	I	CNOT	I $\otimes$ I
0.1%	0.1%	5.6 (4.5)	5.5 (4.6)	5.5 (4.7)	4.4 (4.1)	4.6 (4.3)
1%	1%	5.6 (2.8)	5.5 (2.7)	5.6 (2.7)	3.7 (2.4)	4.2 (2.3)
5%	5%	5.3 (1.4)	5.3 (1.2)	5.4 (1.1)	3.2 (1.1)	4.0 (0.9)

TABLE I. Robust fidelities for the single-qubit and two-qubit gates on the building blocks of Fig. 2, calculated at three levels of uncertainty in  $\Delta J$  and  $\Delta g$ . The uncertainty in the detuning is kept at  $\Delta\delta/\bar{J} = 0.1\%$ . The maximum amplitude of the Rabi frequencies is constrained to less than  $10\bar{J}$ . I and I  $\otimes$  I are the identity gates for the driven subsets of the four-qubit and six-qubit building block, respectively. The gate duration is  $T = 2\pi/\bar{J}$ , divided into  $M = 100$  time bins. The figures shown are the exponents of the infidelity, i.e.,  $-\log_{10}(1 - \mathcal{F}_{\max})$ , which is the number of nines in  $\mathcal{F}_{\max}$ . The figures inside the bracket are results obtained with non-robust optimization.

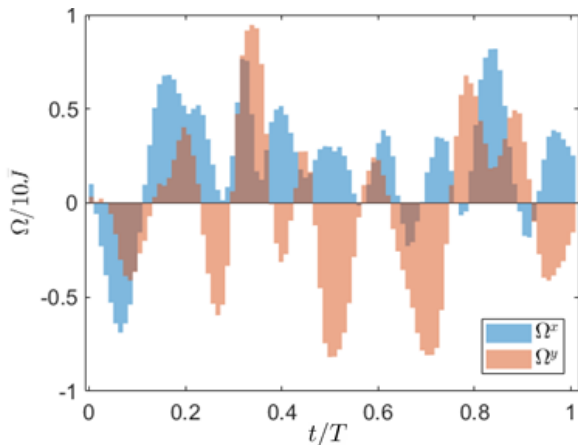


FIG. 3. Optimal pulse for the Hadamard gate at 1% uncertainty in Table I.

Now we discuss read out for the qubit array. At the end of the computation the drives are turned off and the system evolves according to the background Hamiltonian  $H_0 = \sum_{j,k} J_{j,k} \sigma_j^z \sigma_k^z$ . The final wavefunction can be expanded in the computational basis,  $|\psi_f\rangle = \sum_{j_1, \dots, j_N=0,1} c_{j_1, \dots, j_N} |j_1, \dots, j_N\rangle$ . Since  $H_0$  consists of exclusively  $\sigma^z$  terms,  $|j_1, \dots, j_N\rangle$  is an eigenstate of  $H_0$  and the evolution under  $H_0$  introduces only addition phases in the coefficients  $c_{j_1, \dots, j_N}$ . Thus, if the solution of a computation is encoded in the bit string of the final wavefunction, as is the case for the Shor's algorithm for factoring [26] and the HHS algorithm for solving linear systems [27], the additional phase will not change the result. Therefore, the projective measurement onto the computational basis can be done at any time after the drives are turned off. The same projective measurement can also be used to prepare the system in a random state in the set of  $2^N$  computational basis vectors, if the read-out fidelity is high enough. From the measurement result one knows exactly this state; and it can be used as the starting point of the computation.

A promising physical realization of our model is the superconducting qubits. An effective ZZ coupling between transmons through their common interaction with a cavity was already demonstrated experimentally [21], and very recently via a flux-tunable coupler [18, 19]. There are also many proposals on realizing ZZ coupling between superconducting qubits for the quantum simulation of interacting spin systems [28, 29]. Our result will serve as another motivation for these proposals. In addition, ZZ coupling is the natural interaction in a nuclear magnetic resonance quantum computer [30], for which sophisticated pulse-shaping is available [31], making it a good test bed for our model. We note that, in NMR quantum computation, the unwanted ZZ couplings are effectively removed by a series of refocusing single-qubit  $\sigma^x$  gates applied in a specific pattern [32]. This necessitates to, in advance, compute the protocol of pulsing for each proposed sequence of gates, resulting in a significant com-

putational overhead when the system is scaled up. The refocusing gates also have to be much stronger than the ZZ coupling, which in practice can mean relatively weak couplings and hence slow entangling gates. Our scheme overcome both of these limitations. The influence of the unwanted ZZ couplings on the undriven qubits is cancelled by applying identity gates. This works through the combined effect of the couplings themselves and the drives on the driven qubits. The latter method works regardless of how strong the coupling is. Our scheme also has a remarkable advantage of being robust against uncertainty/inhomogeneity in the qubit's parameters. This reduces overheads in both designing pulses and device calibration.

Although a honeycomb array is the focus of this paper, the qubits can be arranged in any physical shape that has the same connectivity, for example a square array with each qubit connected to only three nearest neighbors. Moreover, there exist driving patterns that satisfy the conditions of commutativity and robust control for other geometries such as square arrays and one dimensional chains (see Appendix). One can also envisage a hybrid architecture where clusters of fixed couplers are connected with tunable couplers, making the control easier while still keeping the number of required tunable couplers low. This has the potential for easing the technological difficulties in scaling up a quantum computer for achieving quantum advantage.

To conclude, we find that it is feasible to implement quantum computing with precise operations on a 2D qubit array with exclusively fixed couplers. The protocol involves robust pulses and active identities for the idle times. The quantum gates are robust against significant uncertainty in the qubit-qubit and drive-qubit coupling caused by fabrication imperfection and/or slowly fluctuating fields. The optimal control signals have a limited bandwidth and can therefore lend themselves to straightforward implementation with existing electronics. We have shown that both 1D and 2D geometries are possible with a robust optimization process which can handle the minimal cluster size which is required for each scheme. The proposed scheme shows that scalability can be accelerated with fixed coupling scheme, thus motivating further development of ZZ couplers in different platforms.

## ACKNOWLEDGMENTS

This work is supported by the UK Hub in Quantum Computing and Simulation, part of the UK National Quantum Technologies Programme with funding from UKRI EPSRC grant EP/T001062/1, and the EPSRC strategic equipment grant no. EP/L02263X/1. All the codes and simulation data of this paper are available without restrictions [33].

## Appendix A: Measurement of qubit frequency

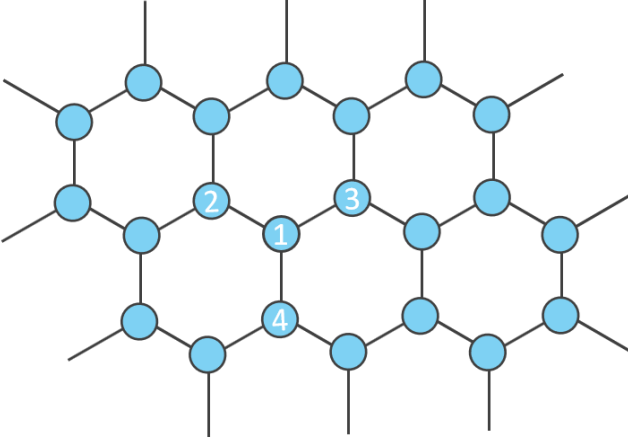


FIG. 4. The frequency of qubit 1 can be determined by one and two-photon absorption measurements on the four qubits of the numbered unit cell (see text).

In this section we propose a procedure using one and two-photon absorption measurements for determining the frequency of every qubits in the 2D honeycomb array. Initially all qubits in the array are in the ground state,  $|0\rangle$ . We want to measure the frequency of qubit 1 in Fig. 4. Due to the ZZ interactions with neighboring qubits causing a dispersive shift the one-photon absorption peak of qubit 1 is at

$$\omega_1^p = \omega_1 - 2(J_{12} + J_{13} + J_{14}). \quad (\text{A1})$$

The shift is the energy cost for flipping three bonds from  $|00\rangle$  to  $|01\rangle$ . Similarly, the one-photon absorption peaks for the other numbered qubits are

$$\begin{aligned} \omega_2^p &= \omega_2 - 2J_{21} - 2 \sum_{\substack{k \in \text{NB}_2 \\ k \neq 1}} J_{2k}, \\ \omega_3^p &= \omega_3 - 2J_{31} - 2 \sum_{\substack{k \in \text{NB}_3 \\ k \neq 1}} J_{3k}, \\ \omega_4^p &= \omega_4 - 2J_{41} - 2 \sum_{\substack{k \in \text{NB}_4 \\ k \neq 1}} J_{4k}, \end{aligned} \quad (\text{A2})$$

where  $\text{NB}_j$  is the set of nearest neighbors of qubit  $j$ . The last sums are the dispersive shifts caused by the ZZ interaction with neighbors that are not qubit 1. Summing all the equations in Eqs. (A1) and (A2), and using  $J_{kl} = J_{lk}$ , one obtains

$$\sum_{j=1}^4 \omega_j^p = \sum_{j=1}^4 \omega_j - 4 \sum_{j=2}^4 J_{1j} - 2 \sum_{j=2}^4 \sum_{\substack{k \in \text{NB}_j \\ k \neq 1}} J_{jk}. \quad (\text{A3})$$

If both qubits 1 and 2 are subjected to the the same field, for example by splitting the field in a Mach-Zehnder

interferometer set-up with one qubit in each arm, one can observe the two-photon transition  $|0\rangle_1 |0\rangle_2 \rightarrow |1\rangle_1 |1\rangle_2$ . Now the coupling energy of the bond between qubit 1 and 2 are not changed, and the two-photon resonance happens at the frequency

$$2\omega_{12}^p = \omega_1 + \omega_2 - 2(J_{13} + J_{14}) - 2 \sum_{\substack{k \in \text{NB}_2 \\ k \neq 1}} J_{2k}, \quad (\text{A4})$$

Similarly, the two-photon resonance frequency for the other qubit pairs are

$$\begin{aligned} 2\omega_{13}^p &= \omega_1 + \omega_3 - 2(J_{12} + J_{14}) - 2 \sum_{\substack{k \in \text{NB}_3 \\ k \neq 1}} J_{3k}, \\ 2\omega_{14}^p &= \omega_1 + \omega_4 - 2(J_{12} + J_{13}) - 2 \sum_{\substack{k \in \text{NB}_4 \\ k \neq 1}} J_{4k}. \end{aligned} \quad (\text{A5})$$

Summing all the equations in Eqs. (A4) and (A5), one obtains

$$2 \sum_{j=2}^4 \omega_{1j}^p = 2\omega_1 + \sum_{j=1}^4 \omega_j - 4 \sum_{j=2}^4 J_{1j} - 2 \sum_{j=2}^4 \sum_{\substack{k \in \text{NB}_j \\ k \neq 1}} J_{jk}. \quad (\text{A6})$$

Finally, subtracting Eq. (A3) from Eq. (A6), the dispersive shifts are cancelled and one arrives at

$$\omega_1 = \sum_{j=2}^4 \omega_{1j}^p - \frac{1}{2} \sum_{j=1}^4 \omega_j^p,$$

which gives the bare frequency of qubit 1 in terms of the one and two-photon resonant frequencies. In most qubit platforms spectroscopic measurements are precise and thus the uncertainty in the qubit's frequency can be very small.

## Appendix B: Decomposable driving pattern for one dimensional chains and square arrays

In the main text we focus on the honeycomb array because it is the 2D graph with the smallest number of nearest neighbors (3), resulting in smallest possible building blocks in 2D. Here we describe how to drive 1D chains and 2D square arrays so that the Hamiltonian can be decomposed into small commuting building blocks. The result is illustrated in the graphs of Fig. 5 where the yellow vertices are driven qubits and cyan vertices undriven ones. For the square array the building block for implementing a target two-qubit gate is thirteen-qubit block where the two-qubit gate can be applied to any two nearest neighbors in the five-qubit driven subset. We could not find a simpler block due to the requirements that both qubits subjected to the two-qubit gate have to be driven, and that for robust control every ZZ link has to

be connected to at least one driven qubit. We found that any driving pattern with a smaller block results in at least one link which is not connected to any driven qubit.

### Appendix C: Calculating fidelity and gradient

We first describe how the fidelity and its gradients are calculated with the midpoint rule. The time duration is divided into  $M$  equal time bins with  $t_0 = 0$  and  $t_M = T$ . The field amplitudes are kept constant during each time bin. The Hamiltonian of a star graph,  $\mathcal{G}$ , at the midpoint of the  $n$ -th interval from  $t_{n-1}$  to  $t_n$  is

$$H_{\mathcal{G},n} = \sum_{j \in \mathcal{C}} \alpha_j [\Omega_{jn} \sigma_j^x + \Omega'_{jn} \sigma_j^y] + \sum_{j,k \in \mathcal{G}} J_{jk} \sigma_j^z \sigma_k^z,$$

where  $\alpha_j$  is a the dimensionless factor introduced to model the uncertainty in the Rabi frequencies (see the Main Text),  $\mathcal{C}$  is the driven subset in the center of the graph and  $J_{jk} \neq 0$  only for nearest neighbors, and

$$\begin{aligned} \Omega_{jn} &= \Omega_{jn}^x \cos(\delta_j(t_n - \Delta t/2)) + \Omega_{jn}^y \sin(\delta_j(t_n - \Delta t/2)), \\ \Omega'_{jn} &= \Omega_{jn}^y \cos(\delta_j(t_n - \Delta t/2)) - \Omega_{jn}^x \sin(\delta_j(t_n - \Delta t/2)), \end{aligned}$$

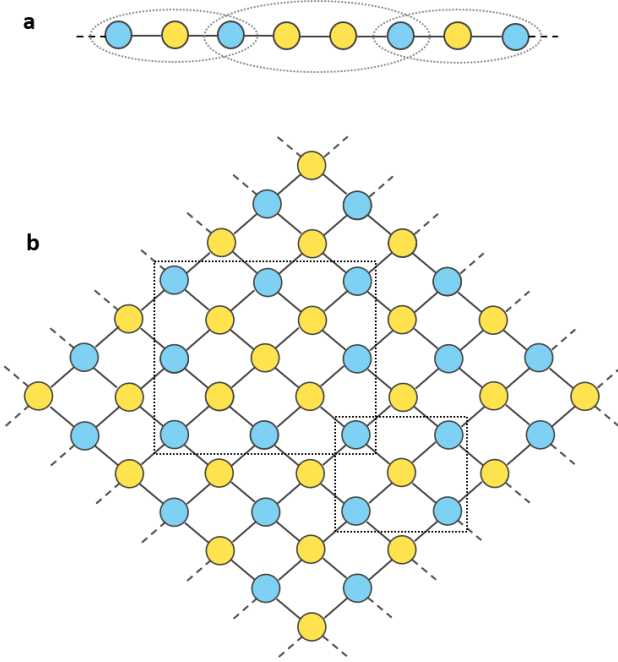


FIG. 5. a) Decomposable driving pattern for a chain: One can implement any single qubit gates on the driving qubit (yellow) of the three-qubit block and any two-qubit gate between the two driving qubits of the four-qubit block. b) Decomposable driving pattern for a square array: single qubit gates can be implemented on the driving qubit of the five-qubit blocks. Two-qubit gates are more complicated in this case due to the condition for robust control (see text), requiring a thirteen-qubit block. A two-qubit gate can be implemented on any two driven qubits in the block.

where  $\Omega_{jn}^{x,y}$  are the Rabi frequencies of the driving field on the  $j$ -th driven qubit during the interval from  $t_{n-1}$  to  $t_n$ . They are the elements of the  $2MN_{\mathcal{C}} \times 1$  control vector,  $\mathbf{c}$ , where  $N_{\mathcal{C}}$  is the number of qubits in the driving subset. The unitary evolution from  $t_{n-1}$  to  $t_n$ ,  $U_n = e^{-iH_{\mathcal{G},n}\Delta t} + O(\Delta t^3)$ , is computed with the expm function in Matlab. For an efficient calculation of the fidelity and the gradients we compute and store all the  $U_n$ , and then obtain the forward and backward unitary propagation operators [24], defined by

$$\begin{aligned} U_n^f &= U_n U_{n-1} \dots U_1, \\ U_{n+1}^b &= U_M U_{M-1} \dots U_{n+1}, \end{aligned}$$

using the recursive relations  $U_n^f = U_n U_{n-1}^f$  and  $U_{n+1}^b = U_{n+2}^b U_{n+1}$ . Then the fidelity is

$$F(\mathbf{c}, \mathbf{v}) = \left| \frac{1}{2^{N_{\mathcal{G}}}} \text{tr} \left[ U_M^{f\dagger} (U_{\mathcal{C}} \otimes I_{\mathcal{B}}) \right] \right|^2,$$

where  $N_{\mathcal{G}}$  is the number of qubits in the star graph.

For computing the gradients we note that

$$H_{\mathcal{G},n} = \sum_{\mu=x,y} \sum_{j \in \mathcal{C}} \Omega_{jn}^{\mu} K_{jn}^{\mu} + \sum_{j,k \in \mathcal{G}} J_{jk} \sigma_j^z \sigma_k^z,$$

where

$$\begin{aligned} K_{jn}^x &= g_j [\sigma_j^x \cos(\delta_j(t_n - \Delta t/2)) - \sigma_j^y \sin(\delta_j(t_n - \Delta t/2))], \\ K_{jn}^y &= \alpha_j [\sigma_j^y \cos(\delta_j(t_n - \Delta t/2)) + \sigma_j^x \sin(\delta_j(t_n - \Delta t/2))]. \end{aligned}$$

One can show that the derivative of  $U_n \equiv e^{-iH_{\mathcal{G},n}\Delta t}$  with respect to  $\Omega_{jn}^{\mu}$  is [24]

$$\frac{\partial U_n}{\partial \Omega_{jn}^{\mu}} = \left\{ -i\Delta t K_{jn}^{\mu} + \frac{\Delta t^2}{2} [H_{\mathcal{G},n}, K_{jn}^{\mu}] \right\} U_n + O(\Delta t^3),$$

where  $[H_{\mathcal{G},n}, K_{jn}^{\mu}]$  is a commutator. It follows that the derivative of  $U_M^f \equiv U_{n+1}^b U_n U_{n-1}^f$  is

$$\frac{\partial U_M^f}{\partial \Omega_{jn}^{\mu}} = U_{n+1}^b \left\{ -i\Delta t K_{jn}^{\mu} + \frac{\Delta t^2}{2} [H_{\mathcal{G},n}, K_{jn}^{\mu}] \right\} U_n^f,$$

and from this it is straight forward to compute the gradient of the fidelity. The most computationally expensive part of the calculation is the matrix exponentiation for obtaining  $U_n$ , which is done  $M$  times.

### Appendix D: Robust optimization

We use two algorithms to raise the worst-case fidelity,  $\mathcal{F}(\mathbf{c})$ , defined in Eq. 4. The first is based on sequential convex programming. We start with initial guesses  $\mathbf{c}_0$  and  $\mathbf{u}_0$  for the control vector and the upper limit (trust region) of the step, respectively. Then a step  $|\delta \mathbf{c}| < \mathbf{u}_0$  is found to maximize  $\min_i \nabla_{\mathbf{c}} F(\mathbf{c}, \mathbf{v}_i) \cdot \delta \mathbf{c}$ , i.e., to maximize

the minimum first-order increment over  $\mathbf{v}_i$ . This ensures all the fidelities at the extreme points of the hypercube,  $\mathcal{V}$ , are increased. The above optimization problem can be solved by sequential convex programming (SCP). We used the YALMIP toolbox and SPDT3 package in Matlab for this purpose. If a step can be found such that  $\min_i \nabla_{\mathbf{c}} F(\mathbf{c}, \mathbf{v}_i) \cdot \delta \mathbf{c}$  is positive then we increase the upper bound  $\mathbf{u}_0$  by 1.15, otherwise we decrease it by 2. We chose these factors as they give the fastest convergence in our numerical tests. The procedure is repeated until either the maximum iteration is reached or the step's upper bound drops below a small tolerance. The second approach is to simply maximize the average fidelity,

$$\bar{F}(\mathbf{c}) = \sum_{i=1}^{n_{\mathcal{X}}} F(\mathbf{c}, \mathbf{v}_i) / n_{\mathcal{X}}, \quad (\text{D1})$$

using a quasi-Newton method. Obviously this does not guarantee that the worst-case fidelity over  $\mathbf{v}$  is increased, as the mean can be increased without increasing the minimum value in the set. However, we found that in our calculations the worst-case fidelity is always improved substantially when we maximize the average fidelity. We optimize  $\bar{F}(\mathbf{c})$  using the interior-point method implemented in Matlab's `fmincon` function, where the Hessian is computed from the exact gradients with the BFGS approximation.

In our numerical tests the first algorithm is more sensitive on the initial guesses of the control parameters. For the two-qubit gates in Table I the computation is very expensive and hence it is not practical to run the optimization with too many initial guesses. We find that for the same running time the second algorithm gives higher fidelities, and the results in Table I are obtained with it.

- 
- [1] F. Arute *et al.*, *Nature* **574**, 505 (2019).
- [2] C. Ballance, T. Harty, N. Linke, M. Sepiol, and D. Lucas, *Physical Review Letters* **117**, 060504 (2016).
- [3] H. Levine, A. Keesling, G. Semeghini, A. Omran, T. T. Wang, S. Ebadi, H. Bernien, M. Greiner, V. Vuletić, H. Pichler, and M. D. Lukin, *Physical Review Letters* **123**, 170503 (2019).
- [4] Y. He, S. K. Gorman, D. Keith, L. Kranz, J. G. Keizer, and M. Y. Simmons, *Nature* **571**, 371 (2019).
- [5] W. Huang, C. H. Yang, K. W. Chan, T. Tanttu, B. Hensen, R. C. C. Leon, M. A. Fogarty, J. C. C. Hwang, F. E. Hudson, K. M. Itoh, A. Morello, A. Laucht, and A. S. Dzurak, *Nature* **569** (2019), 10.1038/s41586-019-1197-0.
- [6] J. M. Nichol, L. A. Orona, S. P. Harvey, S. Fallahi, G. C. Gardner, M. J. Manfra, and A. Yacoby, *npj Quantum Information* **3** (2017), 10.1038/s41534-016-0003-1.
- [7] Y. Chen *et al.*, *Physical Review Letters* **113**, 220502 (2014).
- [8] A. G. Fowler, M. Mariantoni, J. M. Martinis, and A. N. Cleland, *Physical Review A* **86**, 032324 (2012).
- [9] G. Wendin, *Reports on Progress in Physics* **80**, 106001 (2017).
- [10] J. Braumüller *et al.*, *Applied Physics Letters* **108**, 032601 (2016).
- [11] B. E. Kane, *Nature* **393**, 133 (1998).
- [12] J. L. Allen, R. Kosut, J. Joo, P. Leek, and E. Ginossar, *Physical Review A* **95**, 042325 (2017).
- [13] J. L. Allen, R. Kosut, and E. Ginossar, [arXiv:1902.08056 \[cond-mat, physics:quant-ph\]](https://arxiv.org/abs/1902.08056) (2019), arXiv: 1902.08056.
- [14] D. Dong, C. Chen, B. Qi, I. R. Petersen, and F. Nori, *Sci. Rep.* **5**, 7873 (2014).
- [15] M. H. Goerz, F. Motzoi, K. B. Whaley, and C. P. Koch, *NPJ Quantum Information* **3**, 37 (2017).
- [16] D. Egger and F. K. Wilhelm, *Supercond. Sci. Technol.* **27**, 014001 (2013).
- [17] A. W. Cross and J. M. Gambetta, *Phys. Rev. A* **91**, 032325 (2015).
- [18] J. Stehlik, D. Zajac, D. Underwood, T. Phung, J. Blair, S. Carnevale, D. Klaus, G. Keefe, A. Carniol, M. Kumph, M. Steffen, and O. Dial, *Physical Review Letters* **127**, 080505 (2021), publisher: American Physical Society.
- [19] M. C. Collodo, J. Herrmann, N. Lacroix, C. K. Andersen, A. Remm, S. Lazar, J.-C. Besse, T. Walter, A. Wallraff, and C. Eichler, *Phys. Rev. Lett.* **125**, 240502 (2020).
- [20] F. Yan, P. Krantz, Y. Sung, M. Kjaergaard, D. L. Campbell, T. P. Orlando, S. Gustavsson, and W. D. Oliver, *Physical Review Applied* **10**, 054062 (2018), publisher: American Physical Society.
- [21] L. DiCarlo *et al.*, *Nature* **460**, 240 (2009).
- [22] S. W. Jolin, R. Borgani, M. O. Tholén, D. Forchheimer, and D. B. Haviland, *Review of Scientific Instruments* **91**, 124707 (2020).
- [23] J. J. Burnett, A. Bengtsson, M. Scigliuzzo, D. Niepce, M. Kudra, P. Delsing, and J. Bylander, *npj Quantum Information* **5**, 1 (2019).
- [24] P. de Fouquieres, S. Schirmer, S. Glaser, and I. Kuprov, *Journal of Magnetic Resonance* **212**, 412 (2011).
- [25] M. A. Nielsen and I. L. Chuang, *Quantum Computation and Quantum Information*, Vol. 1 (Cambridge University Press, 2000).
- [26] P. W. Shor, *SIAM Journal on Computing* **26**, 1484 (1997).
- [27] A. W. Harrow, A. Hassidim, and S. Lloyd, *Physical Review Letters* **103**, 150502 (2009).
- [28] M. Kounalakis, C. Dickel, A. Bruno, N. K. Langford, and G. A. Steele, *npj Quantum Information* **4**, 1 (2018).
- [29] A. J. Kerman, *New Journal of Physics* **21**, 073030 (2019).
- [30] L. M. K. Vandersypen, M. Steffen, G. Breyta, C. S. Yannoni, M. H. Sherwood, and I. L. Chuang, *Nature* **414**, 883 (2001).
- [31] X.-d. Yang, C. Arenz, I. Pelczer, Q.-M. Chen, R.-B. Wu, X. Peng, and H. Rabitz, *Physical Review A* **102**, 062605 (2020).
- [32] T. Tsunoda, G. Bhole, S. A. Jones, J. A. Jones, and P. J. Leek, *Physical Review A* **102**, 032405 (2020), publisher: American Physical Society.
- [33] Data, to be uploaded to zenodo.